

LTH 614
HU-EP-03/86

DESY 03-205
Edinburgh 2003/24
LU-ITP 2003/032

The nucleon mass in $N_f = 2$ lattice QCD: finite size effects from chiral perturbation theory

A. Ali Khan^a, T. Belyaev^b, M. Göckeler^{c,d}, T.R. Hemmert^e,
R. Horsley^f, A.C. Irving^g, B. Joó^f, D. Pleiter^h, P.E.L. Rakow^g,
G. Schierholz^{h,i}, H. Stüben^j

QCDSF-UKQCD Collaboration

^a*Institut für Physik, Humboldt Universität zu Berlin, D-10115 Berlin*

^b*Joint Institute for Nuclear Research, 141980 Dubna, Russia*

^c*Institut für Theoretische Physik, Universität Leipzig, D-04109 Leipzig, Germany*

^d*Institut für Theoretische Physik, Universität Regensburg, D-93040 Regensburg, Germany*

^e*Physik-Department, Theoretische Physik, Technische Universität München, D-85747 Garching, Germany*

^f*School of Physics, University of Edinburgh, Edinburgh EH9 3JZ, UK*

^g*Theoretical Physics Division, Department of Mathematical Sciences, University of Liverpool, Liverpool L69 3BX, UK*

^h*John von Neumann-Institut für Computing NIC, Deutsches Elektronen-Synchrotron DESY, D-15738 Zeuthen, Germany*

ⁱ*Deutsches Elektronen-Synchrotron DESY, D-22603 Hamburg, Germany*

^j*Konrad-Zuse-Zentrum für Informationstechnik Berlin, D-14195 Berlin, Germany*

Abstract

In the framework of relativistic $SU(2)_f$ baryon chiral perturbation theory we calculate the volume dependence of the nucleon mass up to and including $O(p^4)$. Since the parameters in the resulting finite size formulae are fixed from the pion mass dependence of the large volume nucleon masses and from phenomenology, we obtain a parameter-free prediction of the finite size effects. We present mass data from the recent $N_f = 2$ simulations of the UKQCD and QCDSF collaborations and compare these data as well as published mass values from the dynamical simulations of the CP-PACS and JLQCD collaborations with the theoretical expectations. Remarkable agreement between the lattice data and the predictions of chiral perturbation theory in a finite volume is found.

Key words: Lattice QCD; chiral effective field theory; finite size effects

PACS: 11.15.Ha; 12.38.Gc

1 Introduction

The computation of hadron masses is one of the basic goals of lattice QCD. However, as in the case of other observables, this computation suffers from a number of systematic uncertainties (not including the statistical errors): Lattice spacing and volume are finite, and the quark masses in the simulations are larger than in reality, in the extreme case of the sea quarks in the quenched approximation even infinite. Hence the Monte Carlo results must be supplemented by several extrapolations: the continuum extrapolation $a \rightarrow 0$, the extrapolation to the thermodynamic limit $L \rightarrow \infty$, and the chiral extrapolation sending the quark masses to their physical values.

It is therefore an important issue to study hadron masses as functions of the quark masses or, in order to avoid problems connected with the evaluation of quark masses on the lattice, as functions of the pseudoscalar (“pion”) mass. A suitable tool for investigating the quark-mass dependence of physical observables like hadron masses is chiral perturbation theory (or, more generally, chiral effective field theory). Once one has convinced oneself that chiral perturbation theory is applicable for the masses used in the simulations, one can extract low-energy constants of chiral effective field theory and extrapolate reliably towards the physical masses. Indeed, as has recently been demonstrated, relativistic baryon chiral perturbation theory leads to a good chiral extrapolation function for the nucleon mass [1] connecting available lattice results with the physical value. On the other hand, it is well known that finite size effects can be calculated from the same effective field theories that describe the quark-mass dependence [2,3]: As long as the volume is not too small, the finite size effects originate from pions which “propagate around the spatial box”. This approach leads to the so-called p expansion, valid for small pion masses $m_\pi = O(p)$ and large spatial volumes L^3 with $L^{-1} = O(p)$ such that $m_\pi L = O(p^0)$. In this paper we work out the finite size corrections for the nucleon mass in this framework and present pion and nucleon masses obtained by the UKQCD and QCDSF collaborations in simulations with $N_f = 2$ dynamical fermions. These and other recent nucleon mass data are compared with the formulae from chiral perturbation theory. Preliminary results of our investigation have been presented in Ref. [4]. For similar studies of the pion mass and pseudoscalar decay constants see Refs. [5,6].

2 Finite size effects at $O(p^3)$

We follow Ref. [1] and employ relativistic $SU(2)_f$ baryon chiral perturbation theory as described in Ref. [7]. In this field theory the “elementary” degrees of freedom are the pion and nucleon fields. For the Lagrangian and further

details see Refs. [1,7]. The leading order contribution to the shift of the nucleon mass away from its value in the chiral limit comes from the piece in the $O(p^2)$ Lagrangian that breaks chiral symmetry explicitly. The next-to-leading order (NLO) contribution, i.e. the $O(p^3)$ contribution, is generated by the one-loop graph (a) of Fig. 1.

The leading one-loop formula for the nucleon mass reads (in the infinite volume)

$$m_N = m_0 - 4c_1 m_\pi^2 + \left[e_1^r(\lambda) + \frac{3g_A^2}{64\pi^2 f_\pi^2 m_0} \left(1 - 2 \ln \frac{m_\pi}{\lambda} \right) \right] m_\pi^4 - \frac{3g_A^2}{16\pi^2 f_\pi^2} m_\pi^3 \sqrt{1 - \frac{m_\pi^2}{4m_0^2}} \left[\frac{\pi}{2} + \arctan \frac{m_\pi^2}{\sqrt{4m_0^2 m_\pi^2 - m_\pi^4}} \right]. \quad (1)$$

Here and in the following, the constants g_A , f_π , ... are to be taken in the chiral limit, m_0 denotes the nucleon mass in the chiral limit, and the quark mass has been replaced by the pion mass m_π using the Gell-Mann-Oakes-Renner relation. The pion decay constant f_π is normalised such that its physical value is 92.4 MeV. The counterterm $e_1^r(\lambda)$ is taken at the renormalisation scale λ , which makes the result (1) scale independent.

Expanding in powers of m_π (up to logarithms) we find

$$m_N = m_0 - 4c_1 m_\pi^2 - \frac{3g_A^2}{32\pi f_\pi^2} m_\pi^3 + \left[e_1^r(\lambda) - \frac{3g_A^2}{64\pi^2 f_\pi^2 m_0} \left(1 + 2 \ln \frac{m_\pi}{\lambda} \right) \right] m_\pi^4 + \frac{3g_A^2}{256\pi f_\pi^2 m_0^2} m_\pi^5 + O(m_\pi^6). \quad (2)$$

In Ref. [1] it was shown that this expansion is a good approximation of the full expression (1). Note, however, that all the terms $\propto m_\pi^3$, m_π^4 , ... in Eq. (2) are of the same chiral order.

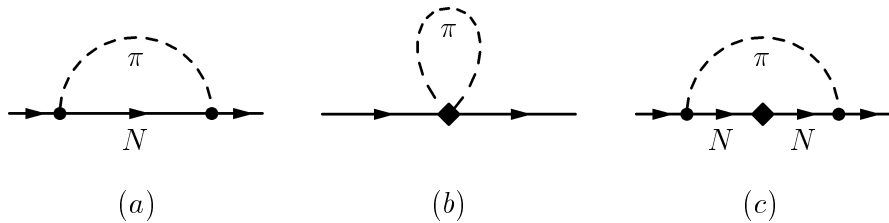


Fig. 1. One-loop graphs of NLO (a) and NNLO (b, c) contributing to the nucleon mass shift. The solid circle denotes a vertex from the leading order Lagrangian, the diamond a vertex from the $O(p^2)$ Lagrangian.

At $O(p^3)$ the volume dependence of the nucleon mass comes from graph (a) in Fig. 1. The corresponding contribution to the nucleon mass reads in Minkowski

space

$$m_a = -i \frac{3g_A^2 m_0 m_\pi^2}{2f_\pi^2} \int_0^\infty dx \int \frac{d^4 p}{(2\pi)^4} [p^2 - m_0^2 x^2 - m_\pi^2 (1-x) + i\epsilon]^{-2}. \quad (3)$$

After a Wick rotation this becomes in Euclidean notation

$$m_a = D \int_0^\infty dx \int \frac{d^4 p}{(2\pi)^4} [p^2 + m_0^2 x^2 + m_\pi^2 (1-x)]^{-2} \quad (4)$$

with

$$D = \frac{3g_A^2 m_0 m_\pi^2}{2f_\pi^2}. \quad (5)$$

In a finite spatial volume of linear size L (the time direction is left infinite) the integral over the spatial components of the loop momentum \vec{p} is replaced by a sum over the discrete set of momenta allowed by the boundary conditions. Since we use periodic boundary conditions, the allowed momenta are of the form $\vec{p} = (2\pi/L)\vec{\ell}$, where $\vec{\ell}$ is a vector with integer components. Hence we get for the difference between the nucleon mass in a volume of size L^3 and the infinite volume nucleon mass at $O(p^3)$

$$\begin{aligned} m_N(L) - m_N(\infty) &= \Delta_a(L) = \\ &= D \int_0^\infty dx \int \frac{dp_4}{2\pi} \left[\frac{1}{L^3} \sum_{\vec{p}} (\vec{p}^2 + p_4^2 + m_0^2 x^2 + m_\pi^2 (1-x))^{-2} \right. \\ &\quad \left. - \int \frac{d^3 p}{(2\pi)^3} (\vec{p}^2 + p_4^2 + m_0^2 x^2 + m_\pi^2 (1-x))^{-2} \right]. \end{aligned} \quad (6)$$

According to Ref. [3] the difference between the sum and the integral is finite and given by

$$\begin{aligned} &\frac{\Gamma(r)}{L^3} \sum_{\vec{p}} (\vec{p}^2 + M^2)^{-r} - \frac{\Gamma(r)}{(2\pi)^3} \int d^3 p (\vec{p}^2 + M^2)^{-r} \\ &= \sum_{\vec{n}}' (4\pi)^{-3/2} \int_0^\infty d\lambda \lambda^{r-5/2} \exp(-\lambda M^2 - L^2 \vec{n}^2 / (4\lambda)), \end{aligned} \quad (7)$$

where the sum extends over all vectors \vec{n} with integer components excluding $\vec{n} = \vec{0}$. Here n_i can be interpreted as the number of times the pion crosses the “boundary” of the lattice in the i direction. With the help of

$$\int_0^\infty d\lambda \lambda^a e^{-\lambda M^2 - b/\lambda} = 2 \left(\frac{b}{M^2} \right)^{(1+a)/2} K_{1+a}(2\sqrt{bM^2}) \quad (8)$$

(see formula 3.471.9 in [8]) we obtain

$$\begin{aligned}
& \frac{\Gamma(r)}{L^3} \sum_{\vec{p}} (\vec{p}^2 + M^2)^{-r} - \frac{\Gamma(r)}{(2\pi)^3} \int d^3 p (\vec{p}^2 + M^2)^{-r} \\
&= \frac{1}{4\pi^{3/2}} \sum_{\vec{n}}' \left(\frac{L^2 \vec{n}^2}{4M^2} \right)^{r/2-3/4} K_{r-3/2}(\sqrt{L^2 \vec{n}^2 M^2}),
\end{aligned} \tag{9}$$

where $K_\nu(x)$ is a modified Bessel function. For the numerical evaluation at smaller masses it is more advantageous to use the relation

$$\begin{aligned}
& \frac{\Gamma(r)}{L^3} \sum_{\vec{p}} (\vec{p}^2 + M^2)^{-r} - \frac{\Gamma(r)}{(2\pi)^3} \int d^3 p (\vec{p}^2 + M^2)^{-r} \\
&= \frac{L^{2r-3}}{(4\pi)^r} \int_0^\infty dt t^{r-5/2} \exp\left(-\frac{M^2 L^2}{4\pi} t\right) [S(1/t)^3 - 1]
\end{aligned} \tag{10}$$

with the theta function

$$S(x) = \sum_{n=-\infty}^{\infty} e^{-\pi n^2 x} = \frac{1}{\sqrt{x}} S(1/x). \tag{11}$$

For $r = 2$ we have from (9)

$$\begin{aligned}
& \frac{1}{L^3} \sum_{\vec{p}} (\vec{p}^2 + M^2)^{-2} - \frac{1}{(2\pi)^3} \int d^3 p (\vec{p}^2 + M^2)^{-2} \\
&= \frac{1}{4\pi^{3/2}} \sum_{\vec{n}}' \left(\frac{L^2 \vec{n}^2}{4M^2} \right)^{1/4} K_{1/2}(\sqrt{L^2 \vec{n}^2 M^2}).
\end{aligned} \tag{12}$$

Hence we can write

$$\begin{aligned}
& \Delta_a(L) \\
&= D \int_0^\infty dx \int \frac{dp_4}{2\pi} \cdot \frac{1}{4\pi^{3/2}} \sum_{\vec{n}}' \left(\frac{L^2 \vec{n}^2}{4} \right)^{1/4} (p_4^2 + m_0^2 x^2 + m_\pi^2 (1-x))^{-1/4} \\
&\quad \times K_{1/2} \left(L |\vec{n}| \sqrt{p_4^2 + m_0^2 x^2 + m_\pi^2 (1-x)} \right).
\end{aligned} \tag{13}$$

Using

$$\int_{-\infty}^\infty dx (x^2 + a^2)^{-1/4} K_{1/2}(b\sqrt{x^2 + a^2}) = \sqrt{\frac{2\pi}{b}} K_0(ab) \tag{14}$$

(see formula 6.596.3 in [8]) we obtain finally

$$\begin{aligned}
& m_N(L) - m_N(\infty) = \Delta_a(L) \\
&= \frac{3g_A^2 m_0 m_\pi^2}{16\pi^2 f_\pi^2} \int_0^\infty dx \sum_{\vec{n}}' K_0 \left(L |\vec{n}| \sqrt{m_0^2 x^2 + m_\pi^2 (1-x)} \right).
\end{aligned} \tag{15}$$

This is the complete $O(p^3)$ result for the volume dependence of the nucleon mass in relativistic baryon chiral perturbation theory. Note that the finite volume has not introduced any new parameter.

3 Finite size effects at $O(p^4)$

At $O(p^4)$, the nucleon self-energy receives additional contributions from graphs (b) and (c) in Fig. 1. Up to higher-order corrections, the contribution to the nucleon mass from graph (c) is cancelled by the contribution arising from the insertion of $m_N = m - 4c_1 m_\pi^2$ in the $O(p^3)$ piece corresponding to graph (a). Alternatively, one could replace the mass m in the free Lagrangian by $m - 4c_1 m_\pi^2$ and omit graph (c) [7]. Thus only graph (b) is relevant for us. The resulting formula for the nucleon mass in the infinite volume at $O(p^4)$ involves two new coupling constants c_2 and c_3 and reads [1,7]

$$\begin{aligned} m_N = m_0 - 4c_1 m_\pi^2 - \frac{3g_A^2}{32\pi f_\pi^2} m_\pi^3 + & \left[e_1^r(\lambda) - \frac{3}{64\pi^2 f_\pi^2} \left(\frac{g_A^2}{m_0} - \frac{c_2}{2} \right) \right. \\ & \left. - \frac{3}{32\pi^2 f_\pi^2} \left(\frac{g_A^2}{m_0} - 8c_1 + c_2 + 4c_3 \right) \ln \frac{m_\pi}{\lambda} \right] m_\pi^4 \\ & + \frac{3g_A^2}{256\pi f_\pi^2 m_0^2} m_\pi^5 + O(m_\pi^6). \end{aligned} \quad (16)$$

The contribution to the nucleon mass from graph (b) in Fig. 1 is given by

$$m_b = -i \frac{3}{f_\pi^2} \int \frac{d^4 p}{(2\pi)^4} \frac{2c_1 m_\pi^2 - (c_2 + c_3)(p^0)^2 + c_3 \vec{p}^2}{m_\pi^2 - p^2 - i\epsilon} \quad (17)$$

in Minkowski space. After a Wick rotation this becomes in Euclidean notation

$$m_b = \frac{3}{f_\pi^2} \int \frac{d^4 p}{(2\pi)^4} \frac{2c_1 m_\pi^2 + (c_2 + c_3)p_4^2 + c_3 \vec{p}^2}{m_\pi^2 + p^2}. \quad (18)$$

Hence we get an additional contribution to the difference between the nucleon mass in a volume of size L^3 and the infinite volume nucleon mass:

$$\begin{aligned} \Delta_b(L) = \frac{3}{f_\pi^2} \int \frac{d p_4}{2\pi} \left[\frac{1}{L^3} \sum_{\vec{p}} \frac{2c_1 m_\pi^2 + (c_2 + c_3)p_4^2 + c_3 \vec{p}^2}{m_\pi^2 + p_4^2 + \vec{p}^2} \right. \\ \left. - \int \frac{d^3 p}{(2\pi)^3} \frac{2c_1 m_\pi^2 + (c_2 + c_3)p_4^2 + c_3 \vec{p}^2}{m_\pi^2 + p_4^2 + \vec{p}^2} \right]. \end{aligned} \quad (19)$$

With the help of

$$\frac{1}{L^3} \sum_{\vec{p}} 1 - \int \frac{d^3 p}{(2\pi)^3} 1 = 0 \quad (20)$$

we obtain

$$\begin{aligned} \Delta_b(L) = \frac{3}{f_\pi^2} \int \frac{dp_4}{2\pi} \left[\frac{1}{L^3} \sum_{\vec{p}} \frac{(2c_1 - c_3)m_\pi^2 + c_2 p_4^2}{m_\pi^2 + p_4^2 + \vec{p}^2} \right. \\ \left. - \int \frac{d^3 p}{(2\pi)^3} \frac{(2c_1 - c_3)m_\pi^2 + c_2 p_4^2}{m_\pi^2 + p_4^2 + \vec{p}^2} \right]. \end{aligned} \quad (21)$$

Now we can use Eq. (9) to rewrite this result as

$$\begin{aligned} \frac{3}{f_\pi^2} \cdot \frac{1}{4\pi^{3/2}} \sum_{\vec{n}}' \left(\frac{L^2 \vec{n}^2}{4} \right)^{-1/4} \int \frac{dp_4}{2\pi} \frac{(2c_1 - c_3)m_\pi^2 + c_2 p_4^2}{(m_\pi^2 + p_4^2)^{-1/4}} \\ \times K_{-1/2} \left(L |\vec{n}| \sqrt{m_\pi^2 + p_4^2} \right), \end{aligned} \quad (22)$$

and by means of Eq. 6.596.3 in [8] we get the final formula

$$\Delta_b(L) = \frac{3m_\pi^4}{4\pi^2 f_\pi^2} \sum_{\vec{n}}' \left[(2c_1 - c_3) \frac{K_1(L|\vec{n}|m_\pi)}{L|\vec{n}|m_\pi} + c_2 \frac{K_2(L|\vec{n}|m_\pi)}{(L|\vec{n}|m_\pi)^2} \right]. \quad (23)$$

Hence we have

$$m_N(L) - m_N(\infty) = \Delta_a(L) + \Delta_b(L) + O(p^5), \quad (24)$$

where $\Delta_a(L)$ is given in Eq. (15). Eq. (24) represents the complete $O(p^4)$ result for the volume dependence of the nucleon mass in relativistic baryon chiral perturbation theory and will serve as the basis for our numerical studies. Again, the finite volume did not lead to the appearance of additional parameters.

The leading contribution in Eq. (24) comes from the terms with $|\vec{n}| = 1$ corresponding to pions which travel around the spatial box exactly once. In the Appendix we bring this contribution into the “dispersive” form introduced by Lüscher [9], which relates the finite volume effects to the pion-proton forward elastic scattering amplitude. We find

$$\begin{aligned}
& [m_N(L) - m_N(\infty)] \Big|_{\text{leading}} \\
&= \frac{3g_A^2 m_0 m_\pi^2}{16\pi^2 f_\pi^2} \left\{ \frac{\pi}{m_0 L} \exp \left(-m_\pi L \sqrt{1 - \frac{m_\pi^2}{4m_0^2}} \right) \right. \\
&\quad \left. - \frac{1}{m_\pi L} \int_{-\infty}^{\infty} dp \frac{\exp(-m_\pi L \sqrt{1 + p^2})}{1 + 4m_0^2 p^2/m_\pi^2} \right\} \\
&+ \frac{9m_\pi^4}{2\pi^2 f_\pi^2} \left[(2c_1 - c_3) \frac{K_1(m_\pi L)}{m_\pi L} + c_2 \frac{K_2(m_\pi L)}{(m_\pi L)^2} \right] + O(p^5). \tag{25}
\end{aligned}$$

The coefficients $2c_1 - c_3$ and c_2 are related to coefficients in the so-called subthreshold expansion [10]. Unless $m_\pi L$ is rather large, the subleading terms with $|\vec{n}| > 1$ are not negligible.

4 Monte Carlo data

We want to compare our formulae to Monte Carlo data for nucleon masses. As the finite size effects rely essentially on the existence of a “pion cloud” and hence on the presence of sea quarks, such a comparison makes sense only for masses extracted from dynamical simulations. Large scale simulations with two flavours of dynamical quarks are beginning to deliver results, but the quark masses are still rather large, and the continuum limit is not easy to perform reliably, because only a rather small range in the lattice spacing a is covered. Therefore it is not straightforward to set the scale for the simulation results. A popular method is to use the force parameter r_0 [11] for that purpose, because it is expected to depend only weakly on the quark masses. In the following we shall adopt this procedure using $r_0 = 0.5$ fm. However, it must be noted that recently some doubts have been raised on the reliability of this method [12], and it would certainly be advantageous to avoid the scale problem completely by considering dimensionless ratios, e.g., ratios of masses with the pion decay constant and performing the whole analysis for these quantities. Another point of concern is the question of whether the quark masses in the simulations are small enough to justify the application of chiral perturbation theory.

Over the last years, the UKQCD and QCDSF collaborations have generated gauge field configurations with two flavours of dynamical quarks for a variety of quark masses, lattice spacings and volumes. These simulations use the standard Wilson plaquette action for the gauge fields and the non-perturbatively $O(a)$ improved clover action for the fermions. The algorithm employed is the Hybrid Monte Carlo algorithm, which recently could be sped up considerably [13]. Details of the extraction of r_0/a are given in [14].

The computation of the nucleon masses on the configurations generated by UKQCD is also described in Ref. [14]. On the configurations generated by QCDSF a somewhat different procedure has been used. While standard interpolating fields have been employed in both cases, QCDSF has applied Jacobi smearing instead of fuzzing when computing the quark propagators from point sources. The nucleon masses have been obtained by fitting the source and sink smeared correlation function to $A_N \exp[-m_N t] + A_{N^*} \exp[-m_{N^*}(T-t)]$, where N^* is the negative parity partner of the nucleon. The χ^2 was calculated from the diagonal part of the covariance matrix only. But it has been checked that using the full covariance matrix gives consistent results. The fit range was fixed by looking for a region where the results for am_N and am_{N^*} are independent of the fit range.

In addition we use data available in the literature [15,16]. The CP-PACS collaboration [15] works with a renormalisation-group improved gauge action and a mean field improved clover quark action, while the JLQCD collaboration [16] employs the same actions as UKQCD and QCDSF. However, JLQCD uses a slightly different value for the improvement parameter c_{SW} . In Table 1 we present our results including those that have already been published in Ref. [14] (points 2, 3, 9, 10). Relevant data obtained by the CP-PACS and JLQCD collaborations are collected in Table 2. Some important quantities converted to physical units are given in Table 3.

Table 1

Simulation parameters and results from the UKQCD and QCDSF collaborations.

Coll.	β	κ_{sea}	volume	r_0/a	am_π	am_N
1	QCDSF	5.20	0.1342	$16^3 \times 32$	4.077(31)	0.5841(11)
2	UKQCD	5.20	0.1350	$16^3 \times 32$	4.754(40)	0.405(5)
3	UKQCD	5.20	0.1355	$16^3 \times 32$	5.041(40)	0.294(4)
4	UKQCD	5.20	0.13565	$16^3 \times 32$	5.246(51)	0.2470(40)
5	UKQCD	5.20	0.1358	$16^3 \times 32$	5.320(50)	0.2080(70)
6	QCDSF	5.25	0.1346	$16^3 \times 32$	4.737(21)	0.4925(16)
7	UKQCD	5.25	0.1352	$16^3 \times 32$	5.138(45)	0.3842(16)
8	QCDSF	5.25	0.13575	$24^3 \times 48$	5.430(60)	0.2599(15)
9	UKQCD	5.26	0.1345	$16^3 \times 32$	4.708(52)	0.509(2)
10	UKQCD	5.29	0.1340	$16^3 \times 32$	4.813(45)	0.577(2)
11	QCDSF	5.29	0.1350	$16^3 \times 32$	5.227(37)	0.4208(8)
12	QCDSF	5.29	0.1355	$12^3 \times 32$	5.756(33)	0.3637(48)
13	QCDSF	5.29	0.1355	$16^3 \times 32$	5.560(30)	0.3334(15)
14	QCDSF	5.29	0.1355	$24^3 \times 48$	5.566(20)	0.3265(6)
						0.6857(35)

Table 2

Simulation parameters and results from the CP-PACS [15] and JLQCD [16] collaborations.

	Coll.	β	κ_{sea}	volume	r_0/a	am_π	am_N
15	CP-PACS	1.95	0.1410	$16^3 \times 32$	3.014(33)	0.42700(98)	1.0532(51)
16	CP-PACS	1.95	0.1400	$16^3 \times 32$	2.821(29)	0.59580(69)	1.2679(39)
17	CP-PACS	1.95	0.1390	$16^3 \times 32$	2.651(42)	0.72857(68)	1.4559(38)
18	CP-PACS	1.95	0.1375	$16^3 \times 32$	2.497(54)	0.89400(52)	1.7035(34)
19	CP-PACS	2.10	0.1382	$24^3 \times 48$	4.485(12)	0.29459(85)	0.7204(42)
20	CP-PACS	2.10	0.1374	$24^3 \times 48$	4.236(14)	0.42401(46)	0.8955(35)
21	CP-PACS	2.10	0.1367	$24^3 \times 48$	4.072(15)	0.51671(67)	1.0226(32)
22	CP-PACS	2.10	0.1357	$24^3 \times 48$	3.843(16)	0.63010(61)	1.1855(26)
23	CP-PACS	2.20	0.1368	$24^3 \times 48$	5.410(21)	0.2785(22)	0.6314(55)
24	CP-PACS	2.20	0.1363	$24^3 \times 48$	5.237(22)	0.3554(10)	0.7349(42)
25	CP-PACS	2.20	0.1358	$24^3 \times 48$	5.073(19)	0.4190(13)	0.8252(47)
26	CP-PACS	2.20	0.1351	$24^3 \times 48$	4.913(21)	0.49996(83)	0.9330(76)
27	JLQCD	5.20	0.1340	$12^3 \times 48$	3.826(50)	0.619(10)	1.153(12)
28	JLQCD	5.20	0.1343	$12^3 \times 48$	4.031(84)	0.5474(51)	1.094(23)
29	JLQCD	5.20	0.1346	$12^3 \times 48$	4.200(56)	0.5011(70)	1.006(24)
30	JLQCD	5.20	0.1350	$12^3 \times 48$	4.481(67)	0.4239(71)	0.915(34)
31	JLQCD	5.20	0.1355	$12^3 \times 48$	5.06(12)	0.328(14)	0.820(36)
32	JLQCD	5.20	0.1340	$16^3 \times 48$	3.880(36)	0.6200(21)	1.166(20)
33	JLQCD	5.20	0.1343	$16^3 \times 48$	4.098(45)	0.5528(40)	1.063(13)
34	JLQCD	5.20	0.1346	$16^3 \times 48$	4.287(58)	0.4939(20)	0.991(14)
35	JLQCD	5.20	0.1350	$16^3 \times 48$	4.621(42)	0.4003(33)	0.828(12)
36	JLQCD	5.20	0.1355	$16^3 \times 48$	5.059(71)	0.2806(64)	0.707(29)
37	JLQCD	5.20	0.1340	$20^3 \times 48$	3.946(30)	0.61630(55)	1.1566(26)
38	JLQCD	5.20	0.1343	$20^3 \times 48$	4.143(29)	0.55270(62)	1.0626(23)
39	JLQCD	5.20	0.1346	$20^3 \times 48$	4.336(50)	0.49020(71)	0.9644(31)
40	JLQCD	5.20	0.1350	$20^3 \times 48$	4.635(53)	0.40037(55)	0.8252(26)
41	JLQCD	5.20	0.1355	$20^3 \times 48$	5.092(83)	0.27133(72)	0.6468(36)

Table 3

Simulation data converted to physical units using $r_0 = 0.5\text{fm}$.

	a [fm]	L [fm]	$m_\pi L$	m_π [GeV]	m_N [GeV]
1	0.12	1.96	9.3	0.9398(19)	1.7813(66)
2	0.11	1.68	6.5	0.760(11)	1.657(26)
3	0.10	1.59	4.7	0.5849(92)	1.524(25)
4	0.10	1.52	4.0	0.5114(97)	1.400(52)
5	0.09	1.50	3.3	0.437(15)	1.335(70)
6	0.11	1.69	7.9	0.9207(51)	1.768(13)
7	0.10	1.56	6.1	0.7791(76)	1.629(20)
8	0.09	2.21	6.2	0.5570(69)	1.320(19)
9	0.11	1.70	8.1	0.946(11)	1.878(28)
10	0.10	1.66	9.2	1.096(11)	2.063(26)
11	0.10	1.53	6.7	0.8681(64)	1.721(14)
12	0.09	1.04	4.4	0.826(12)	1.963(29)
13	0.09	1.44	5.3	0.7316(51)	1.577(19)
14	0.09	2.16	7.8	0.7172(29)	1.5062(94)
15	0.17	2.65	6.8	0.5079(57)	1.253(15)
16	0.18	2.84	9.5	0.6633(69)	1.412(15)
17	0.19	3.02	11.7	0.762(12)	1.523(24)
18	0.20	3.20	14.3	0.881(19)	1.679(36)
19	0.11	2.68	7.1	0.5214(21)	1.2751(82)
20	0.12	2.83	10.2	0.7088(25)	1.4971(77)
21	0.12	2.95	12.4	0.8304(32)	1.6434(79)
22	0.13	3.12	15.1	0.9556(41)	1.7980(85)
23	0.09	2.22	6.7	0.5946(52)	1.348(13)
24	0.10	2.29	8.5	0.7345(37)	1.519(11)
25	0.10	2.37	10.1	0.8389(41)	1.652(11)
26	0.10	2.44	12.0	0.9694(45)	1.809(17)
27	0.13	1.57	7.4	0.935(19)	1.741(29)
28	0.12	1.49	6.6	0.871(20)	1.740(52)
29	0.12	1.43	6.0	0.831(16)	1.667(46)
30	0.11	1.34	5.1	0.750(17)	1.618(65)
31	0.10	1.19	3.9	0.655(32)	1.637(82)
32	0.13	2.06	9.9	0.9494(94)	1.785(35)
33	0.12	1.95	8.8	0.894(12)	1.719(28)
34	0.12	1.87	7.9	0.836(12)	1.677(33)
35	0.11	1.73	6.4	0.7300(90)	1.510(26)
36	0.10	1.58	4.5	0.560(15)	1.412(61)
37	0.13	2.53	12.3	0.9598(74)	1.801(14)
38	0.12	2.41	11.1	0.9037(64)	1.737(13)
39	0.12	2.31	9.8	0.8388(98)	1.650(20)
40	0.11	2.16	8.0	0.7324(84)	1.509(18)
41	0.10	1.96	5.4	0.5453(90)	1.300(22)

5 Comparison with chiral perturbation theory

In this section we confront the nucleon masses presented in the preceding section with chiral perturbation theory. We use data obtained on (relatively) large lattices to find appropriate values for the parameters of the chiral expansion. After fixing these parameters, the finite size formulae predict the volume dependence of the nucleon masses without any free parameter.

In Ref. [1] an analysis of data points from Tables 1 and 2 obtained on (relatively) large and fine lattices has been presented. More precisely, masses from simulations with $a < 0.15$ fm, $m_\pi L > 5$ and $m_\pi < 800$ MeV have been considered. Here we shall impose the same conditions and select the data points 2, 7, 8, 14, 19, 20, 23, 24, 40, 41 for the further analysis. (Point 13, which also fulfills the above criteria, is discarded, because the corresponding simulation parameters agree with those of point 14, except that the lattice is smaller. Similarly, simulations 30 and 35 just repeat simulation 40 on smaller lattices.)

We cannot determine all parameters in the chiral perturbation theory formulae from fits to the lattice data. Therefore we decided to fix g_A , f_π , c_2 , c_3 , and to fit the remaining parameters m_0 , c_1 , $e_1^r(\lambda)$ choosing $\lambda = 1$ GeV. For g_A and f_π we take the physical values $g_A = 1.267$, $f_\pi = 92.4$ MeV. Choosing values for c_2 and c_3 is more difficult, although there are quite a few phenomenological determinations in the literature (see, e.g., [17,18,19,20,21,22]). In particular, c_3 seems to be subject to a considerable uncertainty. We set $c_2 = 3.2$ GeV $^{-1}$, which is compatible with Refs. [17,18,19,22], and consider two possibilities for c_3 : $c_3 = -3.4$ GeV $^{-1}$ and $c_3 = -4.7$ GeV $^{-1}$. According to Ref. [22], the value $c_3 = -3.4$ GeV $^{-1}$ is consistent with the empirical nucleon-nucleon phase shifts and with the value extracted in [20] from pion-nucleon scattering. On the other hand, $c_3 = -4.7$ GeV $^{-1}$ is the central value obtained in the pion-nucleon scattering analysis of Ref. [20], albeit with large error bars..

From a fit of Eq. (16) to the ten points selected above with $c_3 = -3.4$ GeV $^{-1}$ we obtain the results labelled as “Fit 1” in Table 4. Data points and fit are shown in Fig. 2. (Using $g_A = 1.2$, $f_\pi = 88$ MeV as better approximations to the values in the chiral limit does not lead to significant differences.) It is first of all remarkable that the Monte Carlo data obtained by different collaborations with different actions all lie close to a single curve. Thus there seems to be no sign of appreciable lattice artefacts. Secondly, the fit describes the data very well and is at the same time compatible with the physical mass values. Thirdly, the fit parameters take values which are consistent with known phenomenology. In particular, c_1 compares favourably with phenomenological determinations [17,19,20,21]. Repeating the fit with $c_3 = -4.7$ GeV $^{-1}$ leads to the results labelled as “Fit 2” in Table 4, which are farther away from the phenomenological numbers.

Of course, one may doubt the applicability of chiral perturbation theory at the larger pion masses which enter our analysis. On the other hand, we do not have enough results at smaller masses to restrict ourselves to a safer mass range performing the same kind of fits as above. We can, however, constrain the fit by requiring the fit curve to pass through the physical point. We implement this constraint by choosing m_0 such that the condition is satisfied. In this way we eliminate one fit parameter leaving only c_1 and $e_1^r(\lambda = 1 \text{ GeV})$ to be fitted. The reduced number of parameters then allows us to restrict the fit to a smaller number of masses. From such constrained fits to the four data points at the smallest masses (points 8, 19, 23, 41) we get the results labelled as “Fit 3” (with $c_3 = -3.4 \text{ GeV}^{-1}$) and “Fit 4” (with $c_3 = -4.7 \text{ GeV}^{-1}$) in Table 4. While the results of Fit 1 and Fit 3 are well compatible with each other (and with phenomenology), the constraint has a stronger effect for $c_3 = -4.7 \text{ GeV}^{-1}$.

Table 4

Results from the four fits of nucleon mass data as described in the text. The parameter c_3 has been kept fixed.

	$c_3 \text{ [GeV}^{-1}]$	$m_0 \text{ [GeV]}$	$c_1 \text{ [GeV}^{-1}]$	$e_1^r(\lambda = 1 \text{ GeV}) \text{ [GeV}^{-3}]$	χ^2
Fit 1	-3.4	0.89(6)	-0.93(5)	2.8(4)	12.18
Fit 2	-4.7	0.76(6)	-1.25(5)	1.7(5)	11.85
Fit 3	-3.4	0.88(-)	-0.93(4)	3.0(6)	0.29
Fit 4	-4.7	0.87(-)	-1.11(4)	3.2(6)	0.39

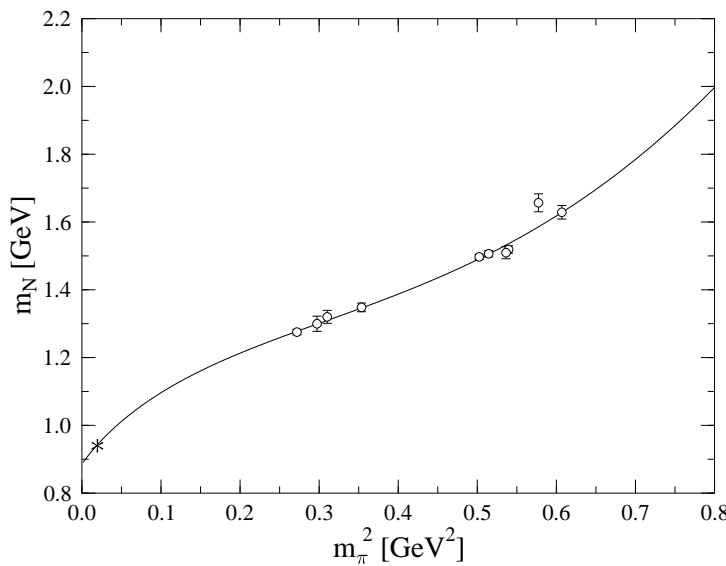


Fig. 2. Nucleon mass data on (relatively) large and fine lattices. The star indicates the physical point. The curve corresponds to Fit 1 in Table 4.

Using the parameters obtained from Fit 1, which are consistent with phenomenology and the large volume Monte Carlo data, we can now evaluate our finite size corrections. Note that no further free parameters are involved. For the comparison with the Monte Carlo results we need data from simulations which differ only in the lattice size while all other parameters are kept fixed. There are six sets of three simulations each among the results in Tables 1, 2. We choose the three sets with the smallest pion masses and plot the nucleon masses versus the lattice size in Figs. 3, 4, 5. The curves are computed from our finite size formulae. The curve labelled p^4 corresponds to

$$m_N(L) = \Delta_a(L) + \Delta_b(L) + m_N(\infty), \quad (26)$$

where $m_N(\infty)$ is determined such that $m_N(L)$ on the largest lattice agrees with the Monte Carlo value. For the pion mass we use the value from the largest lattice. In the curve labelled p^3 , the p^4 contribution $\Delta_b(L)$ has been left out, but $m_N(\infty)$ has not been changed.

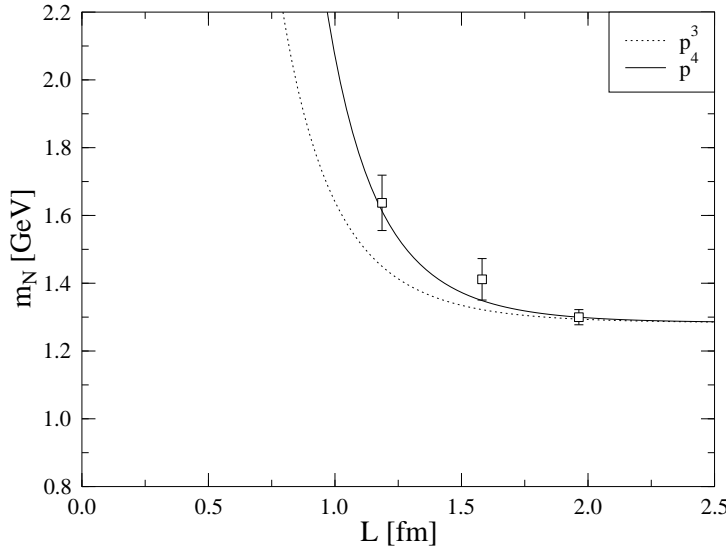


Fig. 3. Volume dependence of the nucleon mass for $m_\pi = 545$ MeV (data points 31, 36, 41). The dotted curve shows the contribution of the p^3 term, while the solid curve includes also the p^4 correction, with the parameters taken from Fit 1.

Our formula describes the volume dependence of the nucleon mass remarkably well. However, the agreement would deteriorate had we taken into account only pions which travel around the lattice exactly once, by restricting the sums over \vec{n} in Eqs. (15), (23) to \vec{n} with $|\vec{n}| = 1$.

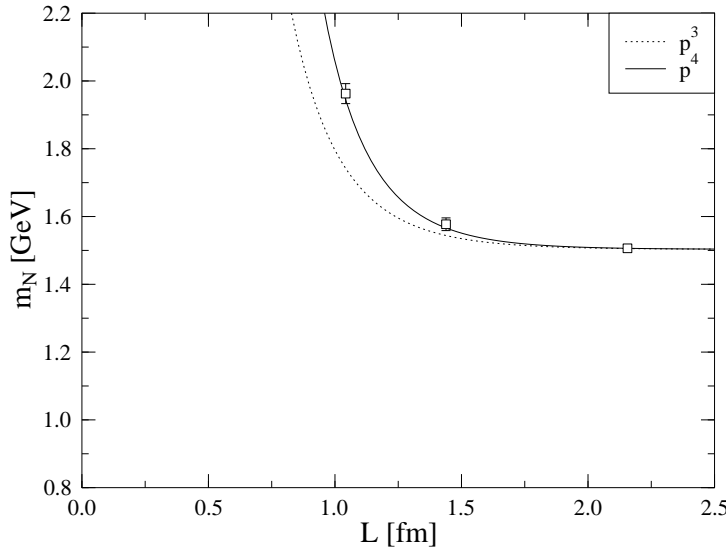


Fig. 4. Volume dependence of the nucleon mass for $m_\pi = 717$ MeV (data points 12, 13, 14). The dotted curve shows the contribution of the p^3 term, while the solid curve includes also the p^4 correction, with the parameters taken from Fit 1.

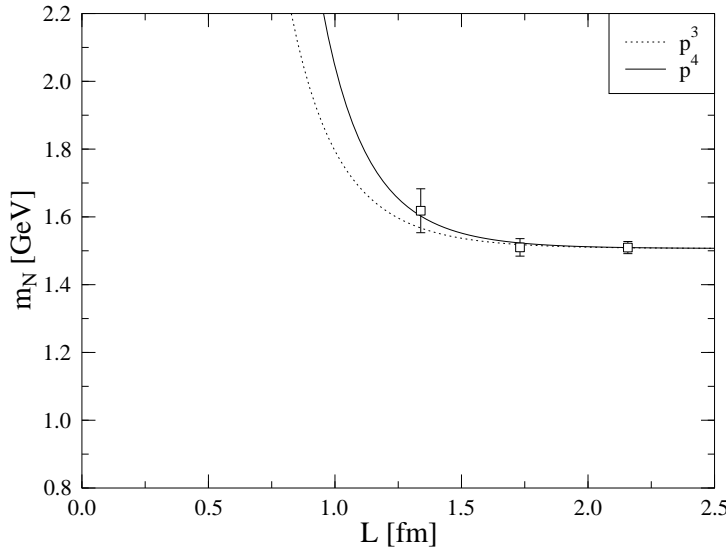


Fig. 5. Volume dependence of the nucleon mass for $m_\pi = 732$ MeV (data points 30, 35, 40). The dotted curve shows the contribution of the p^3 term, while the solid curve includes also the p^4 correction, with the parameters taken from Fit 1.

6 Conclusions

Chiral effective field theories evaluated in a finite volume yield expressions for physical quantities, e.g. masses, in the form of an expansion with an expansion parameter p , where the pion mass m_π and the inverse box size $1/L$ both count as quantities of order p . We have applied this formalism to the nucleon mass using relativistic $SU(2)_f$ baryon chiral perturbation theory up to and including $O(p^4)$ terms.

Setting the scale with $r_0 = 0.5$ fm, we can convert Monte Carlo results obtained in simulations with dynamical quarks to physical units and compare them with our formulae. The infinite-volume formulae lead to a surprisingly good description of the data coming from (relatively) large lattices, with values for the coupling constants of the effective theory which are completely consistent with known phenomenology [1]. Given these coupling constants, there are no free parameters left in the finite size formulae. But the p^4 formulae reproduce the finite size effects observed in the Monte Carlo data surprisingly well. For this agreement it is essential that our formalism incorporates the effects of pions travelling around the lattice arbitrarily many times. Thus we arrive at a more optimistic opinion on the applicability of chiral perturbation theory than previous investigations [23].

We find a remarkably consistent picture of the volume and pion mass dependence of the nucleon mass, in spite of the fact that the “convergence” of the chiral expansion at the rather large pion masses used in the available simulations is far from obvious. Lattice data for smaller masses will therefore be of great importance to corroborate this conclusion. Another point which deserves further investigation is the cutoff and mass dependence of r_0 [12]. Alternatively one could try to avoid the use of r_0 by basing the analysis on ratios of masses with a quantity which is more easily accessible to chiral perturbation theory than r_0 , e.g. the pion decay constant. One could then work out formulae directly for these ratios. Finally it would be interesting to see if the pion mass can be described along similar lines.

Appendix

In this Appendix we compare our description of finite size effects with a finite size formula derived by Lüscher [9]. He expresses the leading contributions to the relative finite size effect

$$\delta_N = (m_N(L) - m_N(\infty)) / m_N(\infty) \quad (27)$$

in terms of the pion-nucleon coupling constant $g_{\pi N}$ with the physical value

$$\frac{g_{\pi N}^2}{4\pi} \approx 14.3 \quad (28)$$

and the pion-proton forward elastic scattering amplitude $F_{\pi p}(\nu)$. Here ν is the “crossing variable” $\nu = (s - u)/(4m_N)$ with $m_N = m_N(\infty)$. Lüscher finds

$$\begin{aligned} \delta_N^{\text{Lüscher}} = & \frac{9}{16\pi m_N L} \left(\frac{m_\pi}{m_N} \right)^2 g_{\pi N}^2 \exp \left(-m_\pi L \sqrt{1 - \frac{m_\pi^2}{4m_N^2}} \right) \\ & - \frac{3}{8\pi m_\pi L} \left(\frac{m_\pi}{m_N} \right)^2 \int_{-\infty}^{\infty} \frac{dp}{2\pi} \exp \left(-m_\pi L \sqrt{1 + p^2} \right) F_{\pi p}(\text{i}m_\pi p) \\ & + O \left(e^{-\alpha m_\pi L} \right), \end{aligned} \quad (29)$$

where $\alpha \geq \sqrt{3/2}$. The amplitude $F_{\pi p}(\nu)$ is related to the amplitude $C^+(\nu) = D^+(\nu)$ of Ref. [10] through

$$F_{\pi p}(\nu) = 6m_N C^+(\nu). \quad (30)$$

It can conveniently be decomposed into the pseudovector Born term and a remainder $R(\nu)$:

$$F_{\pi p}(\nu) = \frac{6g_{\pi N}^2}{1 - 4m_N^2 \nu^2/m_\pi^4} + R(\nu). \quad (31)$$

Using the so-called subthreshold expansion [10] for vanishing momentum transfer

$$R(\nu) = 6m_N \sum_{k=0}^{\infty} d_{k0}^+ \nu^{2k} \quad (32)$$

Lüscher’s formula becomes (ignoring questions of convergence)

$$\begin{aligned} \delta_N^{\text{Lüscher}} = & \frac{9}{8\pi^2} \left(\frac{m_\pi}{m_N} \right)^2 g_{\pi N}^2 \left\{ \frac{\pi}{2m_N L} \exp \left(-m_\pi L \sqrt{1 - \frac{m_\pi^2}{4m_N^2}} \right) \right. \\ & - \frac{1}{m_\pi L} \int_{-\infty}^{\infty} dp \frac{\exp \left(-m_\pi L \sqrt{1 + p^2} \right)}{1 + 4m_N^2 p^2/m_\pi^2} \Big\} \\ & - \frac{9}{4\pi} \frac{m_\pi}{m_N L} \sum_{k=0}^{\infty} m_\pi^{2k} d_{k0}^+ (-1)^k \int_{-\infty}^{\infty} \frac{dp}{2\pi} \exp \left(-m_\pi L \sqrt{1 + p^2} \right) p^{2k} \\ & + O \left(e^{-\alpha m_\pi L} \right). \end{aligned} \quad (33)$$

As it is written, Lüscher’s formula refers to a fixed value of m_π . However, as far as we have information on the quark-mass dependence of m_N , $g_{\pi N}$ and the

scattering amplitude – and chiral perturbation theory provides such information – we can make use of this knowledge to describe the m_π dependence of δ_N as well. But Lüscher's formula takes into account only pions which travel around the lattice exactly once. For the comparison with our formulae we therefore have to restrict the sums over \vec{n} in Eqs. (15), (23) to \vec{n} with $|\vec{n}| = 1$. In order to get the relative finite size effect we must furthermore divide by m_N . Because our finite size formulae correspond to $O(p^3)$ (in the case of Δ_a) and $O(p^4)$ (if also Δ_b is taken into account) in the chiral expansion, we identify here and in the following m_N with m_0 – the higher terms in m_N would give a contribution only at $O(p^5)$. Thus we get from graph (a)

$$\delta_a = \frac{3g_A^2 m_\pi^2}{16\pi^2 f_\pi^2} \int_0^\infty dx \cdot 6 \cdot K_0 \left(L \sqrt{m_0^2 x^2 + m_\pi^2 (1-x)} \right), \quad (34)$$

while graph (b) yields

$$\delta_b = \frac{9}{2\pi^2 f_\pi^2} \frac{m_\pi^4}{m_0} \left[(2c_1 - c_3) \frac{K_1(m_\pi L)}{m_\pi L} + c_2 \frac{K_2(m_\pi L)}{(m_\pi L)^2} \right]. \quad (35)$$

First we consider δ_a and show that the integral over x in (34) can be rewritten as

$$\begin{aligned} & \int_0^\infty dx K_0 \left(L \sqrt{m_0^2 x^2 + m_\pi^2 (1-x)} \right) \\ &= \frac{\pi}{m_0 L} \exp \left(-m_\pi L \sqrt{1 - \frac{m_\pi^2}{4m_0^2}} \right) - \frac{1}{m_\pi L} \int_{-\infty}^\infty dp \frac{\exp(-m_\pi L \sqrt{1+p^2})}{1 + 4m_0^2 p^2/m_\pi^2} \end{aligned} \quad (36)$$

for $m_\pi^2 < 4m_0^2$. We begin by writing

$$\begin{aligned} & \int_0^\infty dx K_0 \left(L \sqrt{m_0^2 x^2 + m_\pi^2 (1-x)} \right) \\ &= \int_{-\infty}^\infty dx K_0 \left(L \sqrt{m_0^2 x^2 + m_\pi^2 (1-x)} \right) \\ & \quad - \int_{-\infty}^0 dx K_0 \left(L \sqrt{m_0^2 x^2 + m_\pi^2 (1-x)} \right). \end{aligned} \quad (37)$$

The first integral on the right-hand side can be evaluated with the help of formula 6.596.3 in [8]:

$$\begin{aligned}
& \int_{-\infty}^{\infty} dx K_0 \left(L \sqrt{m_0^2 x^2 + m_{\pi}^2 (1 - x)} \right) \\
&= \int_{-\infty}^{\infty} dx K_0 \left(L \sqrt{m_0^2 x^2 + m_{\pi}^2 \left(1 - \frac{m_{\pi}^2}{4m_0^2} \right)} \right) \\
&= \frac{\pi}{m_0 L} \exp \left(-m_{\pi} L \sqrt{1 - \frac{m_{\pi}^2}{4m_0^2}} \right). \tag{38}
\end{aligned}$$

In the second integral we use the integral representation

$$K_0(xy) = \int_y^{\infty} ds \left(s^2 - y^2 \right)^{-1/2} e^{-xs} \tag{39}$$

(valid for $x, y > 0$) and interchange the order of the integrations:

$$\begin{aligned}
& \int_{-\infty}^0 dx K_0 \left(L \sqrt{m_0^2 x^2 + m_{\pi}^2 (1 - x)} \right) \\
&= \int_1^{\infty} ds \int_0^{y(s)} dx \left(s^2 - 1 - \frac{m_0^2}{m_{\pi}^2} x^2 - x \right)^{-1/2} e^{-m_{\pi} L s} \tag{40}
\end{aligned}$$

with the abbreviation

$$y(s) = \frac{m_{\pi}}{m_0} \sqrt{s^2 - 1 + \frac{m_{\pi}^2}{4m_0^2}} - \frac{m_{\pi}^2}{2m_0^2}. \tag{41}$$

The integration over x can now be performed leading to

$$\frac{m_{\pi}}{m_0} \int_1^{\infty} ds e^{-m_{\pi} L s} \arctan \left(\frac{2m_0}{m_{\pi}} \sqrt{s^2 - 1} \right). \tag{42}$$

Partial integration yields

$$\frac{2}{m_{\pi} L} \int_1^{\infty} ds \frac{e^{-m_{\pi} L s}}{1 + 4m_0^2(s^2 - 1)/m_{\pi}^2} \cdot \frac{s}{\sqrt{s^2 - 1}}, \tag{43}$$

and the change of variables $s = \sqrt{1 + p^2}$ gives the final expression

$$\int_{-\infty}^0 dx K_0 \left(L \sqrt{m_0^2 x^2 + m_{\pi}^2 (1 - x)} \right) = \frac{1}{m_{\pi} L} \int_{-\infty}^{\infty} dp \frac{\exp \left(-m_{\pi} L \sqrt{1 + p^2} \right)}{1 + 4m_0^2 p^2 / m_{\pi}^2} \tag{44}$$

completing the proof of Eq. (36).

With the help of the Goldberger-Treiman relation

$$g_A = g_{\pi N} \frac{f_{\pi}}{m_0}, \tag{45}$$

which is exact in the chiral limit, we now obtain

$$\delta_a = \frac{9}{8\pi^2} \left(\frac{m_\pi}{m_0} \right)^2 g_{\pi N}^2 \left\{ \frac{\pi}{m_0 L} \exp \left(-m_\pi L \sqrt{1 - \frac{m_\pi^2}{4m_0^2}} \right) - \frac{1}{m_\pi L} \int_{-\infty}^{\infty} dp \frac{\exp \left(-m_\pi L \sqrt{1 + p^2} \right)}{1 + 4m_0^2 p^2 / m_\pi^2} \right\}. \quad (46)$$

The chiral corrections to (45) are of order p^2 and hence would contribute only at $O(p^5)$, beyond the accuracy of our calculation. Thus δ_a reproduces the first two terms in (33) up to a factor of two in the first term, which in Lüscher's treatment originates from nucleon exchange diagrams.

Do the following terms of Eq. (33) contain our δ_b , Eq. (35)? With the help of

$$\int_{-\infty}^{\infty} \frac{dp}{2\pi} \exp \left(-z \sqrt{1 + p^2} \right) p^{2k} = -\frac{1}{\pi} \frac{\Gamma(k + 1/2)}{\Gamma(1/2)} 2^k \frac{d}{dz} z^{-k} K_k(z) \quad (47)$$

and the tree-level relations (see, e.g., Ref. [7])

$$\begin{aligned} d_{00}^+ &= -\frac{2m_\pi^2}{f_\pi^2} (2c_1 - c_3) + O(m_\pi^3), \\ d_{10}^+ &= \frac{2}{f_\pi^2} c_2 + O(m_\pi) \end{aligned} \quad (48)$$

we obtain

$$\begin{aligned} &-\frac{9}{4\pi} \frac{m_\pi}{m_0 L} \sum_{k=0}^{\infty} m_\pi^{2k} d_{k0}^+ (-1)^k \int_{-\infty}^{\infty} \frac{dp}{2\pi} \exp \left(-m_\pi L \sqrt{1 + p^2} \right) p^{2k} \\ &= \frac{9}{2\pi^2 f_\pi^2} \frac{m_\pi^4}{m_0} \left[(2c_1 - c_3) \frac{K_1(m_\pi L)}{m_\pi L} + c_2 \frac{K_2(m_\pi L)}{(m_\pi L)^2} + \dots \right] \end{aligned} \quad (49)$$

in complete agreement with (35).

In short, when we write the $|\vec{n}| = 1$ contributions of our finite size formula (24) in the form that Lüscher uses [9], we find, within the accuracy of our chiral expansion,

$$\begin{aligned} \delta_N &= \frac{9}{8\pi m_N L} \left(\frac{m_\pi}{m_N} \right)^2 g_{\pi N}^2 \exp \left(-m_\pi L \sqrt{1 - \frac{m_\pi^2}{4m_N^2}} \right) \\ &- \frac{3}{8\pi m_\pi L} \left(\frac{m_\pi}{m_N} \right)^2 \int_{-\infty}^{\infty} \frac{dp}{2\pi} \exp \left(-m_\pi L \sqrt{1 + p^2} \right) F_{\pi p}(im_\pi p), \end{aligned} \quad (50)$$

which looks like Lüscher's formula, except that the leading term has a coefficient twice as large. Numerically this makes a significant difference (more than

a factor 2) because in Lüscher's case the exponential and the integral almost cancel each other.

Acknowledgements

The numerical calculations have been performed on the Hitachi SR8000 at LRZ (Munich), on the Cray T3E at EPCC (Edinburgh) under PPARC grant PPA/G/S/1998/00777, on the Cray T3E at NIC (Jülich) and ZIB (Berlin), as well as on the APE1000 and Quadrics at DESY (Zeuthen). We thank all institutions for their support.

This work has been supported in part by the European Community's Human Potential Program under contract HPRN-CT-2000-00145, Hadrons/Lattice QCD and by the DFG (Forschergruppe Gitter-Hadronen-Phänomenologie). A. A.K. thanks the DFG for a research grant (No. AL 596/1). We are also thankful for the support provided by the ECT* (Trento). Discussions with A. Schäfer and W. Weise are gratefully acknowledged. TRH thanks the Institute for Theoretical Physics of the University of Regensburg, the Institute for Physics of the Humboldt University Berlin and DESY Zeuthen for their kind hospitality.

References

- [1] M. Procura, T.R. Hemmert and W. Weise, hep-lat/0309020.
- [2] J. Gasser and H. Leutwyler, Phys. Lett. B184 (1987) 83; *ibid.* B188 (1987) 477; Nucl. Phys. B307 (1988) 763.
- [3] P. Hasenfratz and H. Leutwyler, Nucl. Phys. B343 (1990) 241.
- [4] A. Ali Khan, T. Biskeyev, M. Göckeler, R. Horsley, A.C. Irving, D. Pleiter, P. Rakow, G. Schierholz and H. Stüben, Nucl. Phys. B (Proc. Suppl.) 119 (2003) 419; A. Ali Khan, T. Biskeyev, M. Göckeler, T.R. Hemmert, R. Horsley, A.C. Irving, D. Pleiter, P.E.L. Rakow, G. Schierholz and H. Stüben, hep-lat/0309133; hep-lat/0312029.
- [5] G. Colangelo, S. Dürr and R. Sommer, Nucl. Phys. B (Proc. Suppl.) 119 (2003) 254; G. Colangelo and S. Dürr, hep-lat/0311023.
- [6] D. Bećirević and G. Villadoro, hep-lat/0311028.
- [7] T. Becher and H. Leutwyler, Eur. Phys. J. C9 (1999) 643.
- [8] I.S. Gradshteyn and I.M. Ryzhik, Table of integrals, series and products (Academic Press, NY, 1980).

- [9] M. Lüscher, in: *Progress in gauge field theory*, eds. G. 't Hooft et al., Cargèse 1983 (Plenum Press, New York, 1984).
- [10] G. Höhler, in *Landolt-Börnstein*, vol. I/9b2, ed. H. Schopper (Springer, Berlin, 1983).
- [11] R. Sommer, *Nucl. Phys.* B411 (1994) 839.
- [12] R. Sommer, S. Aoki, M. Della Morte, R. Hoffmann, T. Kaneko, F. Knechtli, J. Rolf, I. Wetzorke and U. Wolff, [hep-lat/0309171](#).
- [13] M. Hasenbusch and K. Jansen, *Nucl. Phys.* B659 (2003) 299; A. Ali Khan, T. Bakeyev, M. Göckeler, R. Horsley, D. Pleiter, P. Rakow, A. Schäfer, G. Schierholz and H. Stüben, *Phys. Lett.* B564 (2003) 235.
- [14] C.R. Allton, S.P. Booth, K.C. Bowler, J. Garden, A. Hart, D. Hepburn, A.C. Irving, B. Joó, R.D. Kenway, C.M. Maynard, C. McNeile, C. Michael, S.M. Pickles, J.C. Sexton, K.J. Sharkey, Z. Sroczynski, M. Talevi, M. Teper and H. Wittig, *Phys. Rev.* D65 (2002) 054502.
- [15] CP-PACS Collaboration, A. Ali Khan et al., *Phys. Rev.* D65 (2002) 054505; Erratum *ibid.* D67 (2003) 059901.
- [16] JLQCD Collaboration, S. Aoki et al., *Phys. Rev.* D68 (2003) 054502.
- [17] V. Bernard, N. Kaiser and U.-G. Meißner, *Nucl. Phys.* A615 (1997) 483.
- [18] N. Fettes, U.-G. Meißner and S. Steininger, *Nucl. Phys.* A640 (1998) 199.
- [19] M. Mojžiš, *Eur. Phys. J.* C2 (1998) 181.
- [20] P. Büttiker and U.-G. Meißner, *Nucl. Phys.* A668 (2000) 97.
- [21] T. Becher and H. Leutwyler, *JHEP* 0106 (2001) 017.
- [22] D.R. Entem and R. Machleidt, *Phys. Rev.* C66 (2002) 014002.
- [23] M. Fukugita, H. Mino, M. Okawa, G. Parisi and A. Ukawa, *Phys. Lett.* B294 (1992) 380; M. Fukugita, N. Ishizuka, H. Mino, M. Okawa and A. Ukawa, *Phys. Rev.* D47 (1993) 4739; B. Orth, T. Lippert and K. Schilling, [hep-lat/0309085](#).